M. Parlier, R. Valle, L. Perrière
(Onera)

S. Lartigue-Korinek, L. Mazerolles
(ICMPE- CNRS)

E-mail: michel.parlier@onera.fr

Potential of Directionally Solidified Eutectic Ceramics for High Temperature Applications

Directionally solidified eutectic (DSE) ceramics add new potentialities to the advantages of sintered ceramics: a higher strength, almost constant, up to temperatures close to the melting point and a better creep resistance. The microstructure of melt-growth composites (MGC) of ceramic oxides consists in three-dimensional and continuous interconnected networks of single-crystal eutectic phases. After solidification of binary eutectics, the eutectic phases are alumina and either a perovskite or garnet phase. In ternary systems, cubic zirconia is added as a third phase. For very high temperature structural applications such as turbine blades in future aeronautical turbines or thermal power generation systems, the investigation is focused on both binary (Al_2O_3-$Y_3Al_5O_{12}$ (YAG), Al_2O_3-$Er_3Al_5O_{12}$ (EAG) and Al_2O_3-$GdAlO_3$ (GAP)) and ternary (Al_2O_3-YAG-ZrO_2, Al_2O_3-EAG-ZrO_2 and Al_2O_3-GAP-ZrO_2) eutectics. Improving the strength and toughness of DSE ceramics being essential for such practical applications, results concerning the mechanical behavior of these eutectics will be reported after a short presentation concerning microstructure and crystallography. This better knowledge of DSE ceramics has led to the development of a specific Bridgman furnace to produce large crystals and investigate possible applications of DSE ceramics to a new generation of very high temperature gas turbines, e.g. hollow non-cooled nozzles, turbine blades or combustor liner panels.

Introduction

Improving the thermal efficiency of aircraft gas turbines and of thermal power generation systems necessitates the development of new ultra high temperature structural materials. In this context, the use of nickel-based superalloys at temperatures beyond 1150°C will be difficult, despite the various studies performed to increase their heat-resistance. For higher temperatures, sintered ceramic oxides or ceramic matrix composites (CMCs) offer many advantages compared to Ni-based superalloys: a lower density and a better resistance to oxidation and abrasion. Unfortunately, sintered ceramics are brittle and their failure strength decreases at high temperature, whereas the use of ceramic fibers in CMCs is limited by grain growth and reaction processes with the matrix and/or the environment at high temperature. On the contrary, melt-growth composites (MGCs), prepared by unidirectional solidification of oxides from the melt, add new potentialities to the advantages of sintered ceramics and CMCs. Studies performed on eutectic compositions between alumina and rare-earth (RE) oxides have led to *in situ* composites consisting in two entangled three-dimensional and continuous interconnected networks of two single-crystal eutectic phases. After solidification, the eutectic phases are alumina and either a perovskite phase $REAlO_3$ (RE: Gd, Eu) or a garnet phase $RE_3Al_5O_{12}$ (RE: Y, Yb, Er, Dy). In the case of ternary systems, cubic zirconia is added to improve the fracture toughness, this phase being present as a dispersoid. The binary and ternary systems both exhibit outstanding mechanical properties, such as a flexural strength that is constant up to temperatures close to the melting point (no amorphous phase at the interfaces between the different phases), good creep resistance, stability of the microstructure, no chemical reaction between the constituent phases and intrinsic resistance to oxidation [1-12].

This investigation is focused on both binary (Al_2O_3-$Y_3Al_5O_{12}$ (YAG), Al_2O_3-$Er_3Al_5O_{12}$ (EAG) and Al_2O_3-$GdAlO_3$ (GAP)) and ternary (Al_2O_3-YAG-ZrO_2, Al_2O_3-EAG-ZrO_2 and Al_2O_3-GAP-ZrO_2) eutectics. These directionally solidified eutectic (DSE) ceramics were grown from the melt using the floating-zone method (arc image furnace). Studies to control the microstructure have been performed, acting on the processing parameters. The mechanical properties have thus been investigated on the small specimens manufactured through this process [13-22]. In this respect, a biaxial testing disc flexure device has been designed to investigate the crack propagation modes in the various phases and in the interfaces [14, 19, 22]. These observations have been correlated to internal stress calculations and piezo-spectroscopy internal stress measurements [14, 16, 19, 22]. Finally, the creep behavior at high temperatures (1450-1600 °C) has been investigated using compression tests [14, 20, 21]. It has been demonstrated that creep mechanisms evolve with the macroscopic

thermomechanical loading (temperature, stress) and a correlation has been established with the deformation mechanisms observed in the entangled microstructure [14, 20, 21].

The next step has been devoted to establish the feasibility of larger crystals using the Bridgman method, which is more appropriate to obtain a homogeneous microstructure in a larger volume. A specific directional solidification furnace has been developed to produce large crystals with melting temperatures up to 2200 °C and to demonstrate the possibility of direct solidification of turbine blades.

From the very beginning, the entire investigation has been performed in close relation with the CNRS-ICMPE Laboratory [13-22]. This paper is thus aimed at presenting a review of the most representative results obtained in the two laboratories, in order to evaluate the potential of DSE ceramics.

Box 1 - Possible applications of DSE oxides

The possible applications of DSE oxides are based on their high mechanical performances, their specific microstructure and their chemical stability. The main functional applications [3] are aimed at:

- using DSE substrates exhibiting a regular two-phase microstructure, for patterned thin film deposition in the domain of nanotechnology and superconductors,
- manufacturing porous cermets for fuel cells (the porous metallic Ni being obtained through reduction of the NiO phase of binary DSE oxides),
- using an ordered eutectic system as a monolithic bundle of optical waveguides, in the case of optically transparent fibers (selective dissolution of one phase may eventually allow it to be replaced by another material of more suitable optical properties),
- obtaining, through slow solidification, porous bioactive ceramics for human bone replacement …

In the domain of structural materials for very high temperature applications, the use of DSE oxides is envisaged for a new generation of gas turbines operating with inlet temperatures as high as 1700 °C [12]. The applications could be vanes, hollow non-cooled nozzles, eventually, turbine blades and, in the combustion chamber, liner panels (figure B1-01).

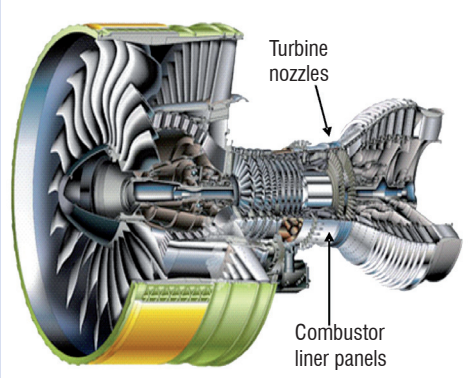

Figure B1-01 - Possible applications for gas turbines: DSE blades, nozzles and vanes, combustor with DSE liner panels. (Although there are no such applications envisaged at present for this type of gas turbine, this picture, available on the Safran-Group Web site, represents the GP 7200 gas turbine designed and developed by Engine Alliance (General Electric and Pratt & Whitney) for Airbus A380, the 9-stage high pressure compressor under the responsibility of Snecma (Safran-Group)).

At the much smaller scale of micro gas turbine engines of power generation machines in the 10 to 100 W electrical power range, the approximately 10 mm in diameter turbine could be machined in DSE oxides [23].

Microstructure and crystallography

Microstructure

Under controlled conditions, solidification from the melt leads to materials free of porosity and with only very few grain boundaries, which are generally at the origin of brittleness in sintered ceramics. The equipment used for the coupled eutectic growth of the oxides consists of high temperature single-crystal growth devices displaying a high thermal gradient. In the present case, rods of oriented eutectics, of about 8 mm in diameter, were grown using the floating-zone translation technique. Solidification runs were achieved in an arc image furnace operating with a 6 kW xenon lamp as a radiation source, at various rates, ranging from 2 to 30 mm h^{-1}.

In most DSE ceramic oxides, coupled growth is mainly controlled by the growth rate. When this rate increases, the eutectic growth undergoes a transition from the homogeneous to the cellular regime that does not correspond anymore to a coupled growth. Scanning Electron Microscopy (SEM) images (figure 1) reveal that the three-dimensional microstructure of the Al_2O_3–YAG eutectic is slightly modified when the growth rate increases; it becomes finer (figure 1 c) and persists up to rates close to 30 mm h^{-1}, before entering into the cellular growth regime (figure 1 d). Similar results were obtained with the other eutectic compositions, thus leading to a selected growth rate of 10 mm h^{-1}.

Box 2 - Coupled eutectic growth

The crucial point leading to the specific microstructure of DSE ceramic composites is the coupled eutectic growth of two (binary eutectics) or three (ternary eutectics) phases from the melt [3]. Let us first consider the **phase diagram** of the Al_2O_3-Gd_2O_3 system at high temperatures (figure B2-01) [24]. The point corresponding to the **lowest temperature** at which the Al_2O_3 and Gd_2O_3 mixture melts or freezes is called the **eutectic point** (Greek ευτηκτος easily melted, from: ευ well and τηκτειν to melt). The corresponding eutectic temperature (T_E) and eutectic composition (C_E) are reported in the phase diagram (figure B2-01). The DSE composite thus obtained through unidirectional solidification is the Al_2O_3/$GdAlO_3$ binary eutectic ceramic composite.

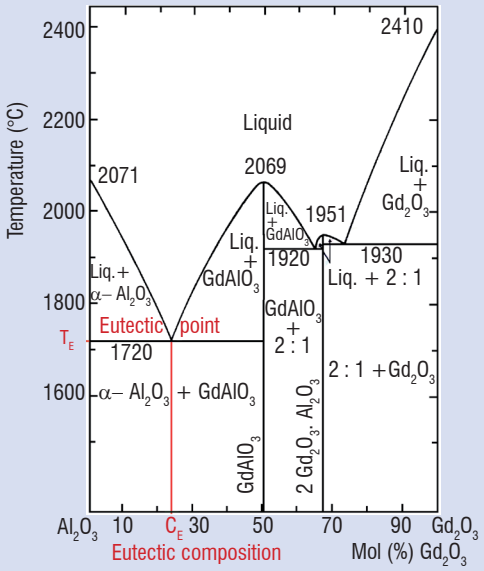

Figure B2-01 - Phase diagram of the Al_2O_3-Gd_2O_3 system at high temperatures [24].

Coupled eutectic growth avoiding the formation of dendrites is a very complex process [3, 25], which implicates numerous phenomena. The entire process will however be briefly and roughly summarized in order to identify the role of the various involved parameters. For the sake of simplicity, although the DSE eutectics present a 3-D interconnected microstructure, a regular lamellar growth (such as that of the well-known Pb-Sn soldering alloy) will be considered (figure B2-02).

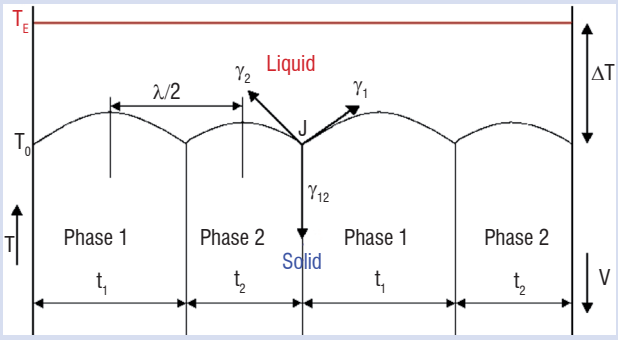

Figure B2-02 – A typical regular lamellar eutectic microstructure growing unidirectionally (V: growth rate)

In this simple case (figure B2-02), the lamellae grow unidirectionally, side by side, and are perpendicular to the planar growth front (solid/liquid interface). Firstly, if the two phases are supposed to grow separately, then long-range diffusion is necessary to ensure **solute transport in the direction of growth.** Secondly, during growth, the solid phase 1 will reject in the liquid phase, atoms corresponding to phase 2 and vice-versa (diffusion coupling), thus leading to a **diffusion flux parallel to the growth front**. The eutectic growth is thus largely governed by **diffusive mass transport**.

At the three-phase junction (J), the **curvature** of the solid phase in contact with the liquid (solid/liquid interface) is determined by the condition of mechanical equilibrium of the **interface forces** (phase 1/phase 2 (γ_{12}), phase 1/liquid (γ_1) and phase 2/liquid (γ_2); arrows in figure B2-02), a phenomenon called **capillarity effects**. In this respect, a specific aspect of ceramics should be emphasized: the capillarity of an oxide such as Al_2O_3 [26] is sufficiently high to allow the growth of commercial sapphire fibers through capillary tubes [27, 28].

These two phenomena, diffusion (through the mean solute undercooling) and capillarity (through the mean curvature undercooling), are the main factors contributing to the ΔT **undercooling** (growth temperature T_0, as compared to the eutectic temperature T_E ($T_0 < T_E$), figure B2-02). Another consequence of these two factors is that the **lamellar spacing** λ (i.e. the size of the microstructure) varies as a function of the growth rate, V (figure B2-02 and figure 1). Concerning the solidification process, the eutectic behaves like a pure chemical substance; due to **latent heat**, the phase change from liquid to solid occurs with a "thermal arrest" (solidification time) in the cooling curve, the internal energy being higher in the liquid than in the solid. In this respect, another specific aspect of ceramic oxides should be noted: the latent heat (also known as specific melting heat or **enthalpy of fusion**) is very high. For instance, in the case of Al_2O_3, the enthalpy of fusion is as high as 111.4 kJ/mol (1092 kJ/kg) [29], instead of 7.15 kJ/mol (60.2 kJ/kg) for Sn, 4.77 kJ/mol (23.04 kJ/kg) for Pb or 6.01 kJ/mol (333.55 kJ/kg) for water, which is well-known for its high enthalpy of fusion. Such a high latent heat may have a non-negligible effect on the **kinetic** undercooling, which depends on the **growth rate** V [3] and constitutes a third contribution to the global ΔT undercooling (figure B2-02). Moreover, material characteristics should also be taken into account, essentially the marked tendency of the two phases to grow under **specific crystallographic orientations** (figure 5). Finally, due to the effects of the various parameters mentioned earlier, such as the coefficient of diffusion (D) of solute in the liquid phase, coupled eutectic growth under a given growth rate V can only be obtained if the **thermal gradient** (G_T) in the ceramic ingot attains a sufficient value. Consequently, coupled eutectic growth is only possible if the ratio G_T/V is higher than a critical value $(G_T/V)_{Critical}$

$$G_T/V > (G_T/V)_{Critical} \qquad \text{(B2-01)}$$

Consequently, in the Bridgman furnace, where the temperature gradient is much smaller than that attained in the floating-zone method, a lower growth rate leads to coupled eutectic growth.

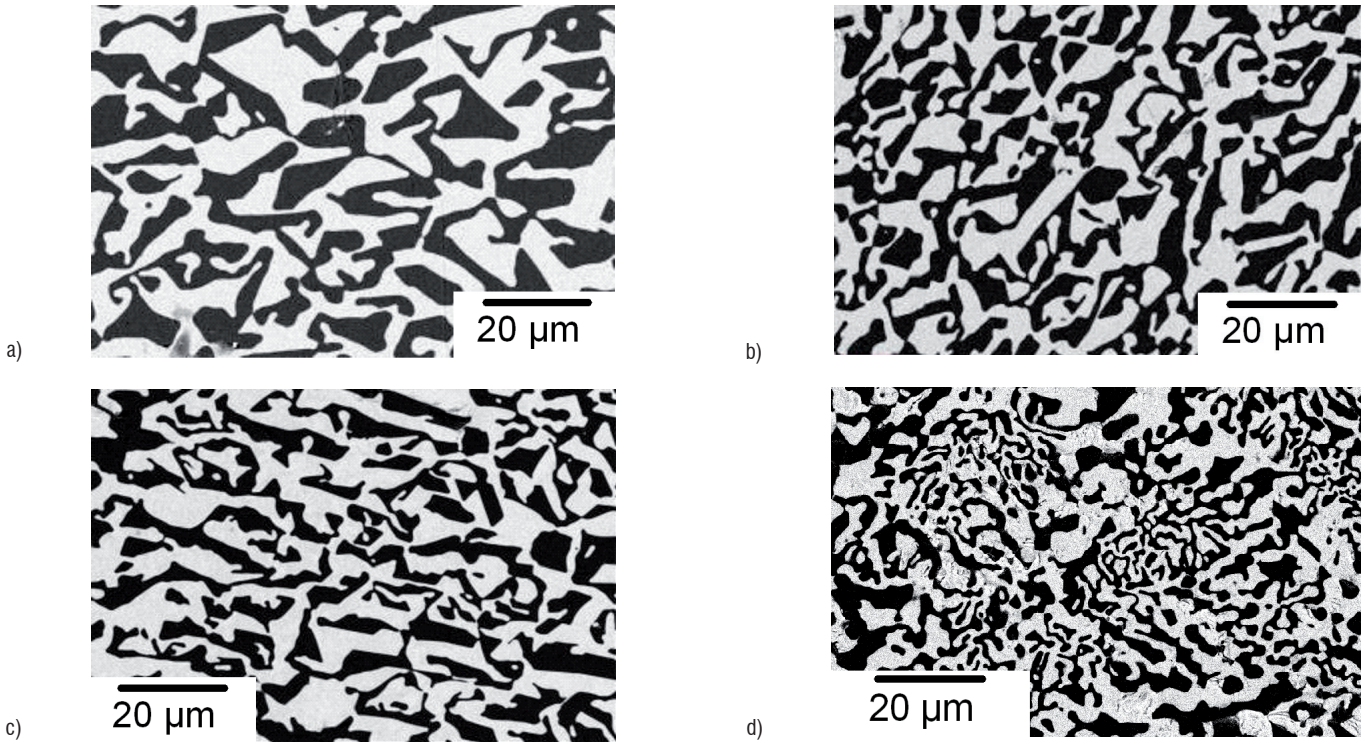

Figure 1 - Back-scattered SEM micrographs of the Al_2O_3–YAG ($Y_3Al_5O_{12}$) eutectic composite (Al_2O_3: dark contrast). Morphology of microstructure *vs.* the solidification rate: 5 mm h^{-1} (a), 12 mm h^{-1} (b), 20 mm h^{-1} (c) and 30 mm h^{-1} (d).

SEM images of the microstructures in cross-sections perpendicular to the solidification direction of binary eutectics are shown in figure 2. In each case, continuous networks of two single-crystal phases are observed: Al_2O_3 (dark contrast) and a perovskite (P) or garnet (G) phase (bright contrast). The domain mean size of each phase (length of the shortest axis) is similar for the Al_2O_3-EAG and Al_2O_3-GAP eutectics (figure 2 b and c), whereas it is much larger for the Al_2O_3–YAG eutectic composites (figure 2 a). Moreover, the Al_2O_3-EAG and Al_2O_3-GAP eutectics exhibit curved interfaces (figure 2 b and c); on the contrary, the Al_2O_3–YAG eutectic composite displays a faceted microstructure with large planar interfaces (figure 2 a).

The same morphology of continuous networks of two single-crystal phases is observed on sections parallel to the growth direction (figure 3). It should be noted that the phases are not elongated in the growth direction, but perfectly similar in shape and size in sections

parallel or perpendicular to the growth direction, thus revealing the three-dimensional configuration of the microstructure (figure 3). The two phases interpenetrate without grain boundaries, pores or colonies.

Typical microstructures of transverse sections of ternary eutectics are shown in figure 4. First of all, it should be noted that the morphology of the garnet-type phase (YAG or EAG) is modified depending on the rare-earth oxide added to alumina and zirconia. The Al_2O_3-YAG-ZrO_2 ternary eutectic displays a fine microstructure with curved smooth interfaces (figure 4 a), instead of the coarser microstructure with large planar interfaces and sharp angles observed in the Al_2O_3–YAG binary eutectic (figure 2 a). In the Al_2O_3-YAG-ZrO_2 ternary eutectic, the cubic zirconia phase grows essentially at the interface between Al_2O_3 and YAG. In the case of Al_2O_3-EAG-ZrO_2 and Al_2O_3-GAP-ZrO_2 ternary eutectics, zirconia dispersoids are observed, not only at the interfaces, but also in the alumina phase (more clearly evidenced at a higher magnification, in figure 6, reporting crack propagation modes in ternary eutectics).

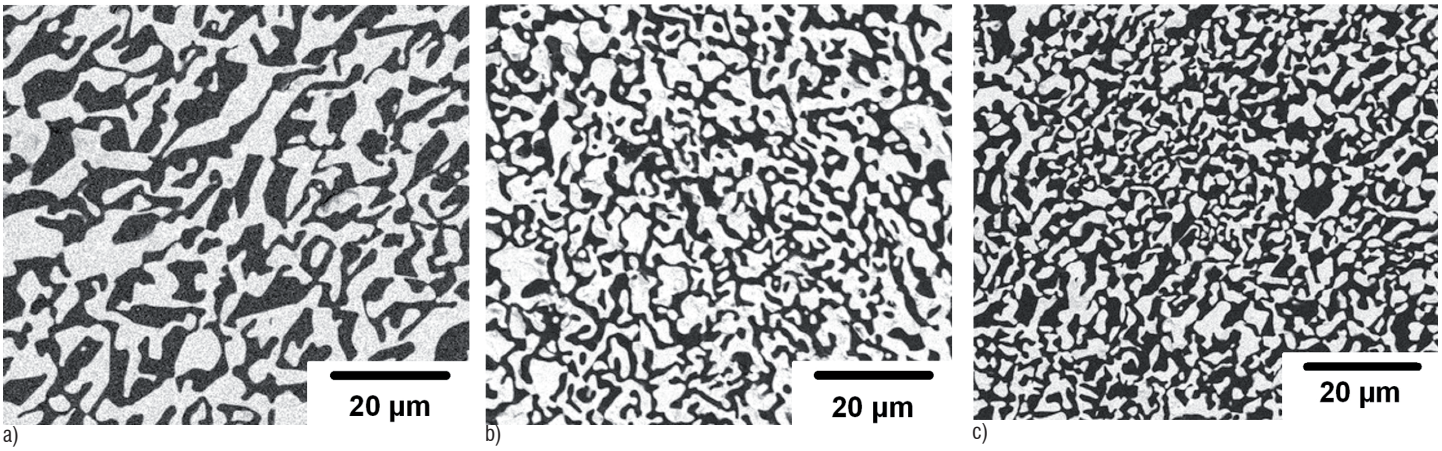

a) b) c)

Figure 2 - Back-scattered SEM micrographs of the transverse sections of binary eutectics showing the continuous three-dimensional interconnected microstructure consisting of Al_2O_3 (dark contrast) and: YAG = $Y_3Al_5O_{12}$ (a), EAG = $Er_3Al_5O_{12}$ (b) and GAP = $GdAlO_3$ (c).

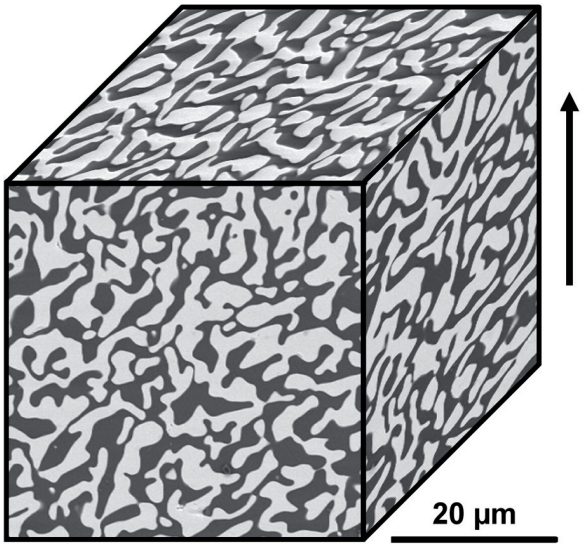

Figure 3 – SEM micrographs revealing the three-dimensional configuration of the microstructure of the Al_2O_3-GAP eutectic composite. The growth direction is indicated by the vertical arrow.

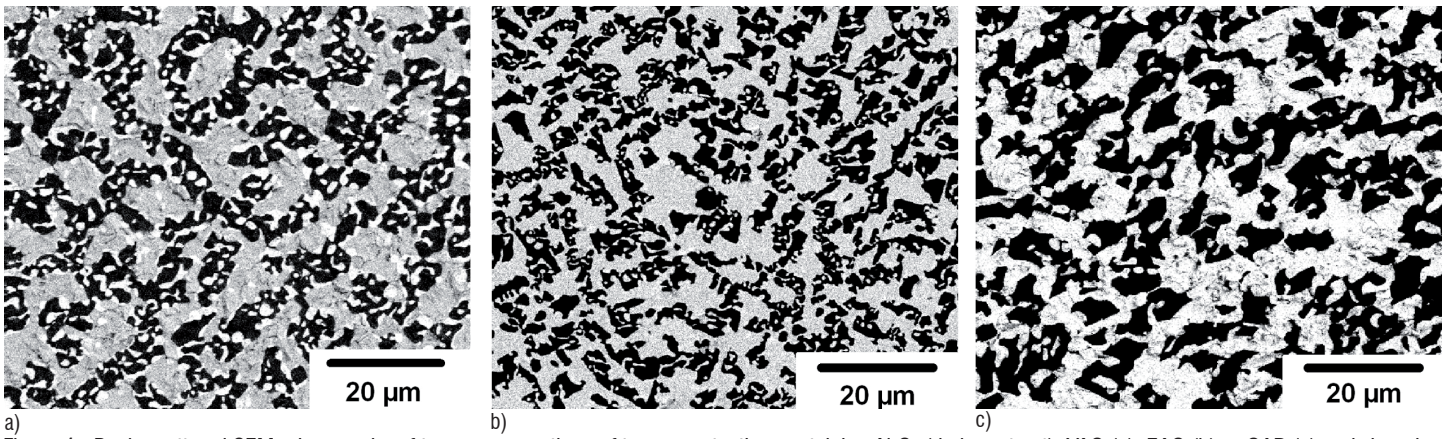

a) b) c)

Figure 4 - Back-scattered SEM micrographs of transverse sections of ternary eutectics containing Al_2O_3 (dark contrast), YAG (a), EAG (b) or GAP (c) and zirconia (bright contrast dots).

Crystallography

Aligned eutectic microstructures (lamellae, fibers, etc.), grown by unidirectional solidification, usually consist of single-crystal phases growing preferentially along well-defined crystallographic directions. These directions are not necessarily the directions of easy-growth of the isolated components, but often correspond to minimum interfacial energy configurations between phases. The perfect crystal lattices of each phase are related by orientation relationships which are unique in most systems and produce well-defined interface planes corresponding to dense atomic arrangements in the component phases. Although the DSE do not display 1-D or 2-D aligned microstructures but 3-D interconnected microstructures, electron diffraction studies performed in Transmission Electron Microscopy (TEM) on thin plates cut perpendicularly to the solidification axis reveal growth directions also corresponding to well-defined crystallographic directions (table 1).

Eutectic phases	Al_2O_3 - Perovskite	Al_2O_3 - Garnet
Growth directions	$[10\bar{1}0]$ Al_2O_3 //[110] Perovskite	$[10\bar{1}0]$ Al_2O_3 //[110] Garnet
Orientation relationships	$(2\bar{1}\bar{1}0)$ Al_2O_3 //(001) Perovskite	(0001) Al_2O_3 //$(1\bar{1}\bar{2})$ Garnet

Table 1 - Growth directions and orientation relationships of the directionally solidified eutectic composites (TEM).

These results, obtained from Selected Area Electron Diffraction (SAED) patterns correspond to analyzed regions of a few micrometers in size; in order to control the single-crystal homogeneity over larger areas, the Electron Back-Scattered Diffraction (EBSD) technique was used [13, 17, 18]. Figure 5 shows the Pole Figures (PF) and the Inverse Pole Figure (IPF) maps for the Al_2O_3–YAG eutectic ceramics (section perpendicular to the growth direction). The orientation maps presented in figure 5 a reveal the sample texture and the nearly single crystal homogeneity of the sample. Each color corresponds to one crystallographic direction, as indicated in the reference stereographic triangles (figure 5 a, right). For example, if YAG crystals had their $<111>$ axis normal to the specimen surface, then they would appear as blue and so on. A unique color corresponds to the YAG phase, which thus exhibits only one growth direction (figure 5 a, bottom). Two different colors are visible for alumina (figure 5 a, top); this is due to the fact that the $[10\bar{1}0]$ and $[0\bar{1}10]$ growth directions are not equivalent in the rhombohedral symmetry, thus resulting in two twin-related variants of Al_2O_3. Moreover, the pole figures (figure 5 b) comfirm the orientation relationship between the two phases: $(0001)_{Al2O3}$ // $(1\bar{1}\bar{2})_{YAG}$.

Concerning the interfaces between alumina, perovskite, garnet and zirconia, atomic scale High Resolution Transmission Electron Microscopy (HRTEM) investigations have revealed the absence of an interphase layer [1, 2, 17, 20]. The orientation of the interface with respect to the adjacent phases growing in epitaxy and the mismatch between the lattice parameters result in a regular network of intrinsic defects along the interface. However, in each phase, the stress field resulting from such an interface is so local and so faint that it cannot be detected in conventional TEM, thus assessing a minimum energy configuration of the interfaces.

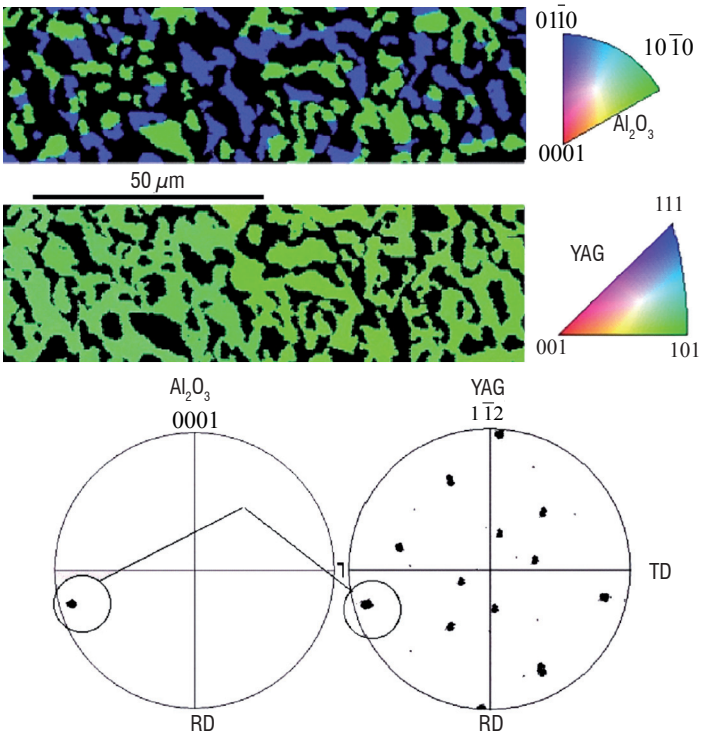

Figure 5 - Inverse Pole Figure maps of Al_2O_3 and YAG phases in a section perpendicular to the growth direction (a) and Pole Figures of 0001_{Al2O3} and $1\bar{1}2_{YAG}$ orientations (b). Orientation relationship: $(0001)_{Al2O3}$ // $(1\bar{1}\bar{2})_{YAG}$ (b).

Mechanical properties

Crack nucleation and propagation modes

Improving the strength and toughness of eutectic ceramics requires a better knowledge of the crack propagation modes in such an interconnected microstructure. In this respect, a biaxial disc flexure testing device has been designed and built at Onera [19]. In the six directionally solidified eutectics [19, 22] investigated, the essential propagation mode is transgranular crack propagation (figure 6). A zigzag crack growth with multiple branches is observed in most cases. However, this type of crack propagation does not only result from deflections of the cleavage crack inside each phase, or when crossing phase boundaries, but more essentially from crack deflection in the interfaces themselves. Interface crack propagation is thus observed between Al_2O_3 and YAG (large black arrow in figure 6 a), Al_2O_3 and EAG (large black arrows in figure 6 b), Al_2O_3 and GAP (large black arrow in figure 6 c), Al_2O_3 and ZrO_2 (white arrows in figure 6 a, b and c), YAG and ZrO_2 (sharp black arrow in figure 6 a) and EAG and ZrO_2 (sharp black arrow in Figure 6 b). Crack branching is observed, not only in one of the various phases such as ZrO_2 (split arrow in figure 6 a), but also in the interfaces where crack deflection through debonding has occurred (split arrows in figure 6 c). In most cases, these bifurcation mechanisms lead to stopped cracks (figure 6 a and c).

The various crack propagation modes may be correlated to internal thermal stress measurements and calculations [19]. For instance, the presence of ZrO_2 phases surrounded by a continuous layer of Al_2O_3 (figure 6 b (top right corner) and c (top left corner)) suggests the use of a concentric cylinder model (figure 7 a). The ZrO_2 phases in figure 6 b (top right corner) and c (top left corner) may be

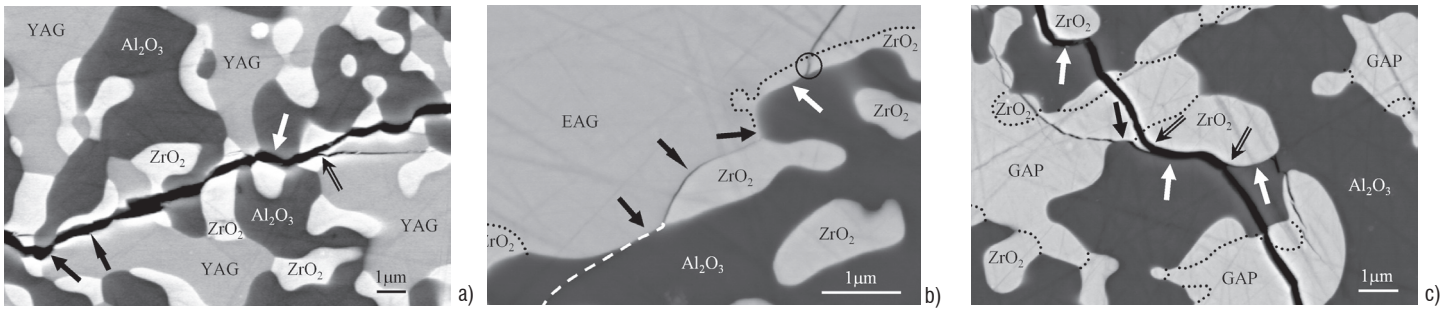

Figure 6 - Crack propagation modes at room temperature in ternary eutectic ceramics subjected to biaxial flexure (Field emission gun (FEG)-SEM, back-scattered electrons): Al_2O_3-YAG-ZrO_2 (a), Al_2O_3-EAG-ZrO_2 (b) and Al_2O_3-GAP-ZrO_2 (c).

represented by a 1 μm in diameter ZrO_2 bar, bonded into a 1.5 μm thick Al_2O_3 sleeve, surrounded by a 0.5 μm thick ZrO_2 sleeve, these three concentric cylinders being embedded into an equivalent homogeneous medium (EHM) having the diameter of the specimen under investigation and the macroscopic thermo-mechanical properties of the bulk Al_2O_3-EAG-ZrO_2 or Al_2O_3-GAP-ZrO_2 eutectics, respectively. In the case of the Al_2O_3-GAP-ZrO_2 eutectics, subjected to a temperature change ($\Delta T \approx 1700°C$), the normal stress ($\sigma_n = \sigma_r$) acting on the ZrO_2-Al_2O_3 interface attains $\approx$ 1000 MPa (figure 7 b); this high tensile normal stress helps interface crack propagation, as observed in figure 6 c (top left corner). The external ZrO_2 layer is subjected to a high tensile circumferential loading ($\sigma_\theta \approx 1800$ MPa) which helps transgranular crack propagation in these phases, as observed in figure 6 b (circle, top right corner) and c (top left corner). As compared to the ultimate tensile strength of such eutectic ceramics [2, 4], the level of these internal thermal stress components is very high, which may explain their essential role in crack nucleation and propagation (e.g. the possibility of crack deflection in the interfaces, in the ternary eutectic ceramics). This high stress level is however in good agreement with the internal stress measurements performed through ruby (Cr^{3+}) fluorescence piezo-spectroscopy [22]. The fact that the observed crack deflection modes are more numerous in ternary than in binary eutectics is in good agreement with the fact that the fracture toughness is improved from the individual constituents, to the binary eutectics ($\approx$ 7 MPa $m^{½}$) and to the ternary eutectics ($\approx$ 10 MPa $m^{½}$) [13, 17].

Moreover, factors other than the thermal mismatch stresses, such as the role of the Young's modulus ratio between garnet or perovskite and alumina, as well as the nature of the interfaces, have a non-negligible effect on the crack deflection and propagation modes [22]. Consequently, due to the presence of a two- or three-phase 3-D interconnected microstructure, a highly detrimental crack propagation mode such as transgranular crack propagation in the brittle ceramic phases is drastically limited by energy dissipative crack deflection modes resulting from thermal mismatch stresses, the effects of Young's modulus ratios and the nature of the interfaces between the various phases [19, 22].

Compressive creep behavior

The compressive creep tests performed on the binary and ternary eutectics under consideration were conducted in air within the stress range 50 to 200 MPa and the temperature range 1450 to 1600 °C. The major axis of the parallelepipedic compressive creep specimens was parallel to the solidification direction. After a short primary stage (e.g. strain of about 0.5%), the secondary creep rate is reached [14, 20, 21].

In this investigation, the stress exponent n, and the activation energy Q, which may be derived from equation (B3-01) and are given by equations (B3-02), have been determined through creep tests performed either at a given temperature with load increments or decrements (stress exponent, n), or at a given load with temperature increments or decrements (activation energy, Q). Practically, during a creep test performed on a given specimen at a given temperature, once a secondary stage steady-state regime is attained and the corresponding creep strain rate $\dot{\varepsilon}$ is experimentally determined, the applied stress is increased and once a new steady-state regime is attained, the corresponding $\dot{\varepsilon}$ is determined. Load increments and decrements are thus applied several times, leading to the determination of strain rates at different stress levels (figure 8 a).

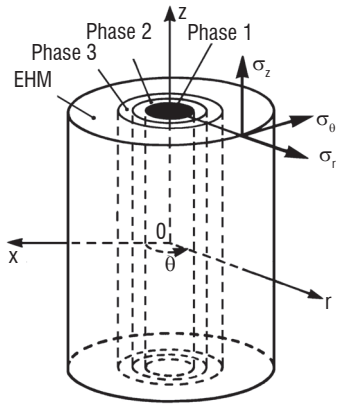

a)

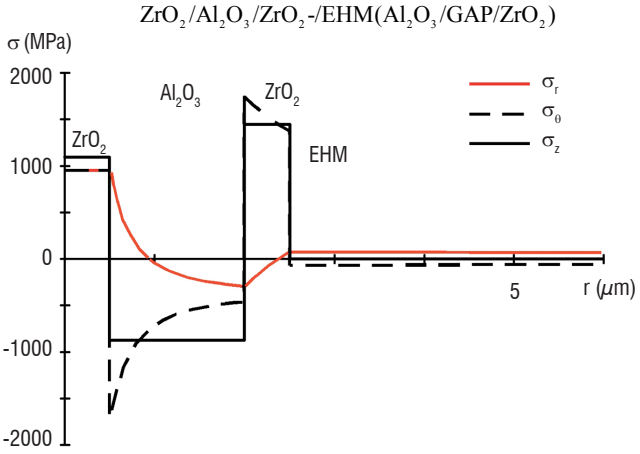

b)

Figure 7 - Internal thermal stresses. The four-phase concentric cylinder model (a), the corresponding stress system (b), where the normal stress σ_n, is given by the radial stress component σ_r.

Box 3 - Creep of ceramics

A good knowledge of the tensile and creep behavior is essential, especially for components subjected to high stresses at high temperatures. Thermomechanical testing of ceramics thus includes tensile tests at various temperatures and high temperature creep tests.

Tensile tests (stress-strain curves) performed at a given temperature and, usually, at a constant strain rate, allow the determination of the elastic and plastic behavior at various temperatures, i.e. Young's modulus (E), the yield stress (Y), the ultimate tensile stress (UTS) and the fracture stress (F).

Creep tests are performed at a constant high temperature but, contrary to tensile tests, the specimen is subjected to a constant high stress loading (**constant load**) during an **extended time period**. Creep tests are thus representative of essential phenomena such as the deformation of turbine blades subjected to centrifugal loading during service, the resulting length extension being detrimental and even totally unacceptable.

In metals, alloys and superalloys, high temperature stress-strain curves and creep curves are usually obtained with standard specimens having a gauge section between two shoulders (the so-called dog-bone-shaped specimens) subjected to a tensile applied loading. Using such a specimen does not only require a large quantity of material, but also necessitates machining of the shoulders of the test specimen, in order to apply the load to the specimen through the grips of the testing system. Although such a device may be successfully used with DSE ceramics (e.g. threaded specimen ends and tapped DSE grips [30]), due to the brittleness of ceramics, the stress-strain curves are usually obtained through three- or four-point bending tests, whereas the creep behavior is studied through **compression creep** tests, as in the present investigation.

The **creep curve** is the representation, as a function of time, of the cumulated creep strain: the "time-dependent" creep strain (figure B3-01). After linear extension of the specimen (elastic behavior), the shape of the creep curve reveals the three stages of creep (figure B3-01). Firstly, the creep strain rate ($\dot{\varepsilon} = d\varepsilon/dt$) decreases (transient creep or primary creep), then the strain rate remains constant over a rather long period (steady-state or secondary creep) and, finally, the strain rate increases, leading to creep rupture of the specimen (accelerating creep or tertiary creep).

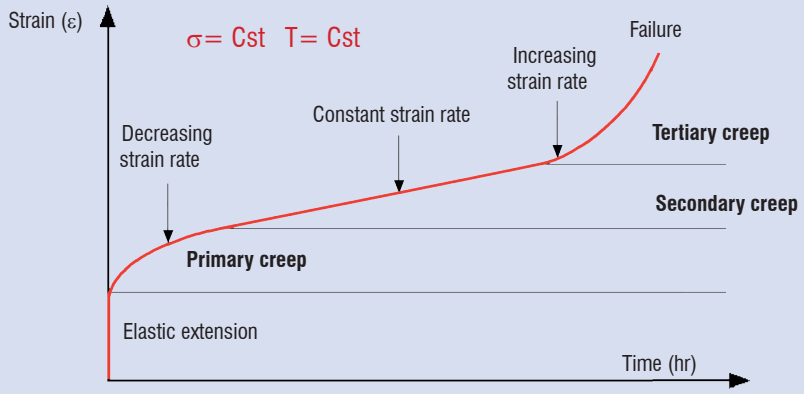

Figure B3-01 – Typical creep curve showing the three stages of the material creep behavior.

In the steady-state (secondary) creep stage, the strain rate ($\dot{\varepsilon}$) is proportional to a power of the applied stress (σ) with a thermal activation term

$$\dot{\varepsilon} = A\,\sigma^{n}\ \exp - Q/RT \qquad \text{(B3-01)}$$

where A is a material constant, n is the stress exponent, Q is the activation energy of the creep mechanism and R and T are, respectively, the gas constant and the absolute temperature.
The stress exponent n, and the activation energy Q, are representative of the creep mechanisms responsible of the creep behavior of the material. Determination of these quantities, in close relation with microstructural investigations, will allow these mechanisms to be identified. These quantities may be derived from equation (B3-01) and are given by

$$n = \left.\frac{\partial \ln \dot{\varepsilon}}{\partial \ln \sigma}\right)_{T,A} \quad \text{and} \quad Q = -R \left.\frac{\partial \ln \dot{\varepsilon}}{\partial l / T}\right)_{\sigma,A} \qquad \text{(B3-02)}$$

However, the determination of these quantities necessitates more complex creep tests to be performed. For instance, creep tests performed at a given temperature (T = Cst), with load increments or decrements, will allow the determination of n (figure 8 a), whereas tests performed under a given loading (σ = Cst), with temperature increments or decrements, will allow the determination of Q (figure 8 b). In both cases, increments or decrements must only be applied once a steady-state regime is attained; the creep strain rate, corresponding to the steady-state regime of each step, may thus be experimentally determined for a given and constant microstructure, the different steps being attained on the same specimen.

In sintered ceramics, due to the presence of numerous grain boundaries and, in most cases, of an amorphous layer at the grain boundaries, high temperature creep may be essentially attributed to diffusion assisted grain boundary sliding. In DSE oxides, the various mechanisms involved in high temperature creep may include thermally activated dislocation motion in the individual phases (glide, cross-slip and climb), bulk (volume) diffusion, etc.

Similarly, creep tests are performed on another specimen at a given stress level and the creep strain rate is determined for each temperature step (figure 8 b) [14, 20, 21].

Although the eutectics under consideration have been thoroughly tested under compressive creep [14], only the more representative results will be reported in this paper (figure 9).

From the results reported in figure 9 a, which are representative of the investigated Al_2O_3-Garnet eutectics [14, 21], it should be noted that, at 1450 °C, the stress exponent (n) increases more rapidly, as the applied stress is increased, than at 1525 °C. Under a low applied stress, a value of n such as 1.14 corresponds to a creep strain rate nearly proportional to the applied stress. Such a value of n suggests a diffusion controlled creep mechanism. At a high stress level and/or high temperature, the value of n is higher ($2<n<3$), which suggests creep mechanisms controlled by dislocation motion.

The creep strain rate *vs.* temperature (1/T) of the Al_2O_3-EAG eutectic composite (figure 9 b) is representative of the investigated Al_2O_3-Garnet eutectics [14, 21]. Concerning the activation energy, the value of $Q \approx 350$ kJ/mol is found only for temperatures lower than 1490 °C and under a low applied stress (70 MPa); the activation energy is otherwise higher: $Q \approx 600$ kJ/mol. Such a high value of Q may correspond to self-diffusion of oxygen atoms in the alumina phase [31]. It should also be noted that similar values have been reported in the literature [32].

In the case of ternary eutectics, the variation of n as a function of the applied stress is similar to that determined in the binary eutectics [14]. Concerning the activation energy (figure 9 c), the value of $Q \approx 400$ kJ/mol is also found for a temperature lower than ≈ 1500 °C in the only case of Al_2O_3-YAG-ZrO_2, a behavior which is similar to that observed in the binary Al_2O_3-Garnet eutectics (figure 9 b). In the other conditions, an activation energy of $Q \approx 600$ kJ/mol has been determined. Concerning the creep strain rates of the ternary eutectics, it should be noted that the behavior of the Al_2O_3-YAG-ZrO_2 and Al_2O_3-GAP-ZrO_2 eutectics is similar to that of the corresponding binary eutectics, whereas that of the Al_2O_3-EAG-ZrO_2 eutectic is lower [14].

Creep tests performed with the compression loading axis perpendicular to the growth direction have revealed a similar creep behavior [21]. This result is essential for structural parts subjected to tension or compression loadings in different directions.

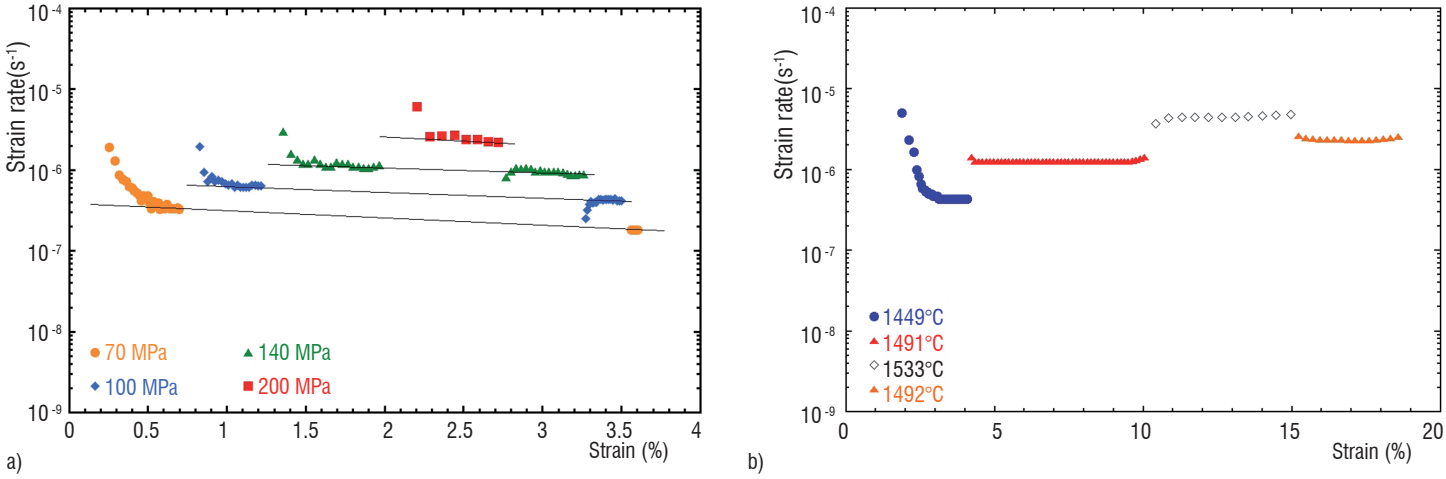

Figure 8 - Compressive creep tests on the Al_2O_3-YAG eutectic composite. Creep strain rate *vs.* strain at 1525°C with stress increments and decrements (a) and creep strain rate *vs.* strain under a 200 MPa loading with temperature increments and decrements (b).

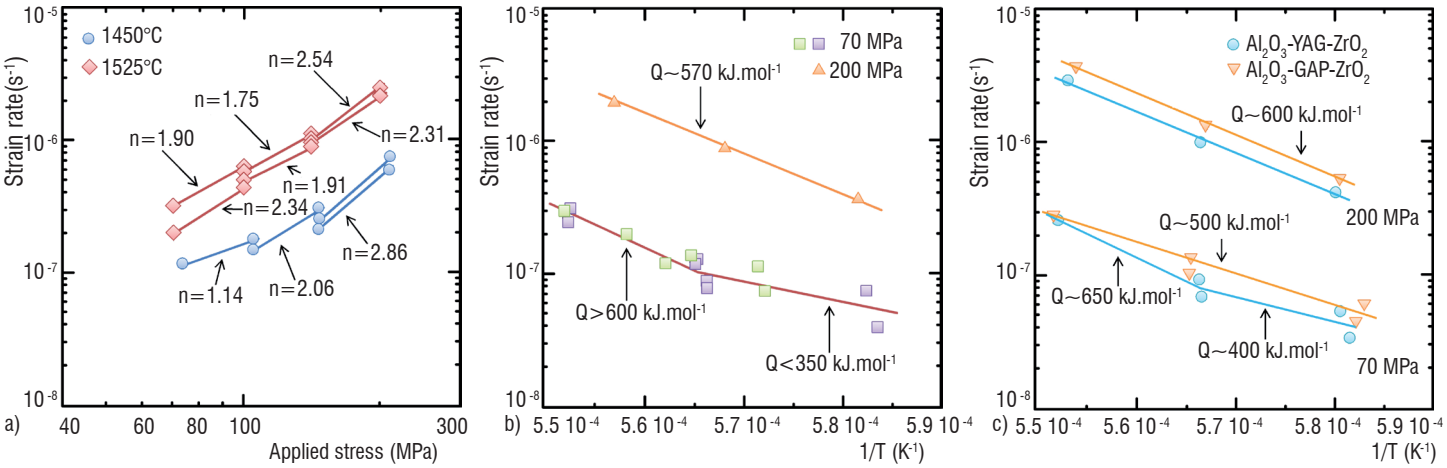

Figure 9 - Compressive creep tests. Creep strain rate νs. applied stress at 1450 °C and 1525 °C for the Al_2O_3-YAG eutectic composite (a). Creep strain rate νs. temperature (1/T) under 70 and 200 MPa loadings for the Al_2O_3-EAG eutectic composite (b). Creep strain rate νs. temperature (1/T) under 70 and 200 MPa loadings for the Al_2O_3-YAG-ZrO_2 and Al_2O_3-GAP-ZrO_2 eutectics (c).

In order to identify the creep deformation modes, transmission electron microscopy (TEM) examinations were performed on specimens previously subjected to compressive creep tests [14, 20, 21]. Due to the strong interface bonding between the various phases, interface sliding mechanisms are nearly impossible. Moreover, due to the difficulty for dislocations to cross the interfaces (difference in lattice parameters), the only possibility to transmit plastic deformation from one phase to the other is to activate a dislocation source in one phase, under the stress concentration resulting from the presence of a dislocation pile-up in the other phase. Otherwise, both phases must deform independently in order to accommodate the global creep deformation. In each phase, the gliding dislocations have to bow within the phase width (λ_P). The shear stress τ necessary for this process is given by

$$\tau = G\mathbf{b}/\lambda_P \qquad (1)$$

where G is the shear modulus and **b** the Burgers vector.

Consequently, when the size of the microstructure decreases (e.g. eutectic morphologies reported in figure 2), the activation of dislocation glide requires higher stresses.

In the alumina phase of the Al_2O_3-GAP eutectics (figure 10 a), the observed dislocations are basal type dislocations ($\mathbf{b} = 1/3[2\bar{1}\bar{1}0]$) aligned in parallel (0001) basal slip planes. This is in agreement with the fact that the basal slip system has the lowest critical resolved shear stress at high temperature [33, 34]. A dislocation pile-up has also been observed in the GAP phase (figure 10 b). This pile-up interacts with the GAP–alumina interface at the bottom of the image, and a basal twin is observed in alumina close to the interaction. Mechanical twinning is probably due to accommodation of the stress concentration resulting from the pile-up.

In the alumina phase of the Al_2O_3-YAG eutectics, rhombohedral dislocations may be observed, thus demonstrating that high stress concentrations may be attained. Thermally activated mechanisms such as dislocation climb have also been observed (figure 10 c, central area). Such a dislocation network, resulting from the reaction of dislocations from the basal and pyramidal slip systems, involves dislocation climb. This diffusion controlled deformation mode was observed in an Al_2O_3-YAG specimen previously subjected to a creep test, for which an activation energy of $Q \approx 670$ kJ/mol was determined. This last result is in good agreement with reference [31], concerning oxygen diffusion controlled mechanisms in alumina.

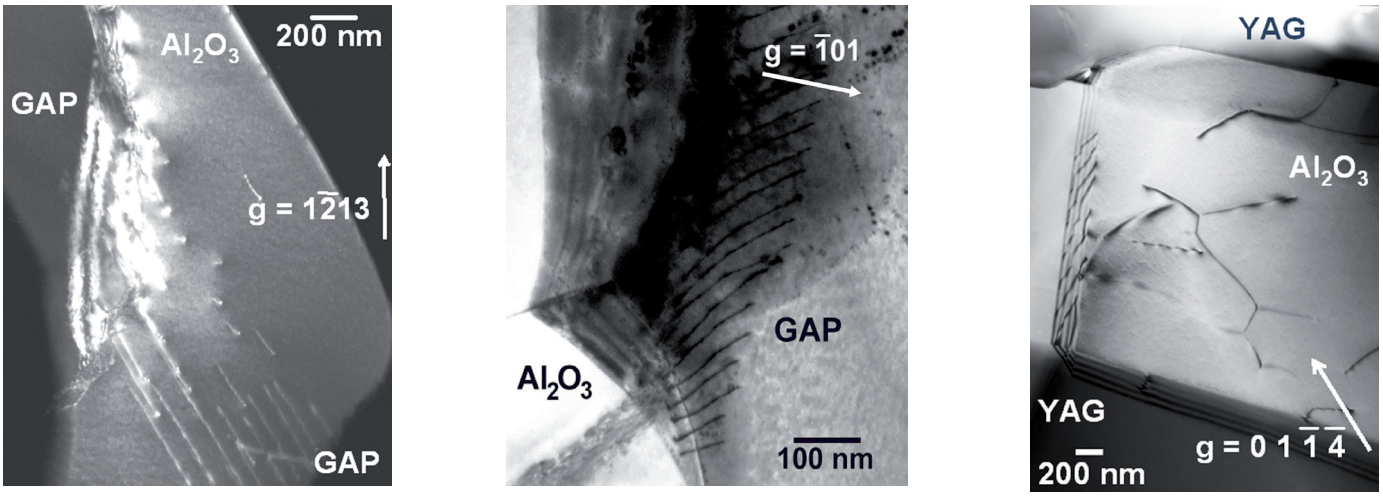

a) b) c)

Figure 10 - TEM examinations of compression tested specimens. Dislocation glide in the Al_2O_3 phase of the Al_2O_3-GAP eutectic composite (a). Dislocation pile-up in the GAP phase of the Al_2O_3-GAP eutectic composite (b). Dislocation reaction involving climb in the Al_2O_3 phase of the Al_2O_3-YAG eutectic composite (c).

The TEM examinations have evidenced plastic deformation of the various phases; furthermore, the different deformation modes thus observed are in good agreement with the stress exponents and activation energies experimentally determined.

Feasibility of turbine blades in a large Bridgman furnace

A large Bridgman furnace has been manufactured (Cyberstar, Grenoble, France) according to the specifications established by Onera (figure 11). This device, which includes two superposed radiofrequency heating elements, ensures a melting zone temperature up to 2200 °C (±1°C) and a crystallization zone temperature up to 1600 °C (±1°C). In the liquid/solid transition zone, a thermal gradient in the range 20 °C/cm to 40 °C/cm is attained. This Bridgman furnace operates either under vacuum or under a neutral atmosphere up to 15 bars and allows a growth rate ranging from 5 to 50 mm h^{-1}. The molybdenum crucible allows the directional solidification of large eutectic crystals up to 50 mm in diameter and 200 mm in height.

Studies in progress concern the determination of the solidification parameters, in order to optimize the microstructure of the Al_2O_3-GAP and Al_2O_3-YAG-ZrO_2 eutectics and their thermomechanical characterization, e.g. flexural strength up to 1500 °C. New eutectic compositions without Al_2O_3 phase will be also investigated, in order to improve the resistance to high temperature water vapor corrosion. Finally, the feasibility of making near net shape turbine blades will be investigated.

Conclusion

Ceramic materials prepared by unidirectional solidification of oxides from the melt are under investigation at Onera, for applications in the aerospace field and in particular for gas turbine blades. Studies to control the microstructure of the directionally solidified eutectic ceramics have been performed and the crystallographic orientation relationships between the constituent phases have been identified. The mechanical properties have been investigated with the aim of understanding the toughening mechanisms and the creep behavior at high temperatures. In the ternary eutectic ceramics, the high level of the internal thermal stresses may explain their essential role in crack nucleation and propagation (e.g. the possibility of crack deflection in the interfaces). The fact that the observed crack deflection modes are more numerous in ternary than in binary eutectics is in good agreement with the improvement of the fracture toughness from the individual constituents, to the binary eutectics and to the ternary eutectics. Concerning the creep strain rates of the ternary eutectics, it should be noted that the behavior of the Al_2O_3-YAG-ZrO_2 and Al_2O_3-GAP-ZrO_2 eutectics is similar to that of the corresponding binary eutectics whereas that of the Al_2O_3-EAG-ZrO_2 eutectic composite is lower. The TEM examinations have evidenced plastic deformation of the various phases; furthermore, the different deformation modes thus observed are in good agreement with the stress exponents and activation energies experimentally determined. This better knowledge of the behavior of DSE ceramics subjected to thermomechanical loadings has led to the development of a specific Bridgman furnace to produce large crystals and near net shape turbine blades. New eutectic compositions without Al_2O_3 phase will be investigated to improve the resistance to high temperature water vapor corrosion ■

a)

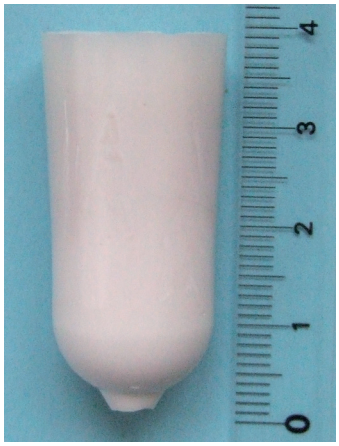

b)

Figure 11 - The Bridgman furnace (a) and an Al_2O_3-$GdAlO_3$ crystal obtained using this furnace (b).

Acknowledgements

The authors would like to thank M. RAFFESTIN (FEG-SEM investigations), D. BOIVIN (EBSD studies), Dr. F. C. LISSALDE (Bridgman furnace, Cyberstar), Dr. L. LIBRALESSO, C. BEN RAMDANE, M. BEJET, J. C. DAUX, S. LALANNE (Bridgman furnace) and Prof. J. CRAMPON for their kind cooperation and fruitful discussions. They would like to express their gratitude to the Regional Council of Île-de-France for the financial support concerning the Bridgman furnace equipment. L. PERRIÈRE would also like to thank the French Defense Research Organization (DGA) for his Doctorate Scholarship.

References

[1] Y. WAKU, N. NAKAGAWA, T. WAKAMOTO, H. OHTSUBO, K. SHIMIZU, Y. KOHTOKU - *A Ductile Ceramic Eutectic Composite with High Strength at 1873 K.* Nature, Vol. 389, pp. 49-52, 1997.

[2] Y. WAKU, N. NAKAGAWA, T. WAKAMOTO, H. OHTSUBO, K. SHIMIZU, Y. KOHTOKU - *High Temperature Strength and Stability of Unidirectionally Solidified Al_2O_3/YAG Eutectic Composite*. J. Mater. Sci., Vol. 33, pp. 1217-1225, 1998.

[3] J. LLORCA, V. M. ORERA - *Directionally Solidified Eutectic Ceramic Oxide*s. Prog. Mater. Sci., Vol. 51, pp. 711–809, 2006.

[4] J. I. PEÑA, M. LARSON, R. I. MERINO, I. DE FRANCISCO, V. M. ORERA, J. LLORCA, J. Y. PASTOR, A. MARTÍN, J. SEGURADO - *Processing, Microstructure and Mechanical Properties of Directionally-Solidified Al_2O_3-$Y_3Al_5O_{12}$-ZrO_2 Ternary Eutectics.* J. Eur. Ceram. Soc., Vol. 26, pp. 3113-3121, 2006.

[5] S. OCHIAI, T. UEDA, K. SATO, M. HOJO, Y. WAKU, N. NAKAGAWA, S. SAKATA, A. MITANI, T. TAKAHASHI - *Deformation and Fracture Behavior of an Al_2O_3/YAG Composite from Room Temperature to 2023 K*. Comp. Sci. Technol., Vol. 61, pp. 2117-2128, 2001.

[6] J. MARTINEZ-FERNANDEZ, A. SAYIR, S. C. FARMER - *High-Temperature Creep Deformation of Directionally Solidified Al_2O_3/$Er_3Al_5O_{12}$*. Acta Mater., Vol. 51, pp. 1705–1720, 2003.

[7] N. NAKAGAWA, H. OHTSUBO, A. MITANI, K. SHIMIZU, Y. WAKU - *High Temperature Strength and Thermal Stability for Melt Growth Composite*. J. Eur. Ceram. Soc., Vol. 25, pp. 1251-1257, 2005.

[8] J. Y. PASTOR, J. LLORCA, A. SALAZAR, P. B. OLIETE, I. DE FRANSISCO, J. I. PEÑA - *Mechanical Properties of Melt-Grown Alumina–Yttrium Aluminum Garnet Eutectics up to 1900 K*. J. Am. Ceram. Soc., Vol. 88, pp. 1488-1495, 2005.

[9] Y. WAKU, S. SAKATA, A. MITANI, K. SHIMIZU, M. HASEBE - *Temperature Dependence of Flexural Strength and Microstructure of Al_2O_3/$Y_3Al_5O_{12}$/ZrO_2 Ternary Melt Growth Composites.* J. Mater. Sci., Vol. 37, pp. 2975–2982, 2002.

[10] J. M. CALDERON-MORENO, M. YOSHIMURA - *Al_2O_3–$Y_3Al_5O_{12}$(YAG)–ZrO_2 Ternary Composite Rapidly Solidified from the Eutectic Melt*. J. Eur. Ceram. Soc., Vol. 25, pp. 1365-1368, 2005.

[11] Y. WAKU, S. SAKATA, A. MITANI, K. SHIMIZU, A. OHTSUKA, M. HASEBE - *Microstructure and High-Temperature Strength of Al_2O_3/$Er_3Al_5O_{12}$/ZrO_2 Ternary Melt Growth Composite*. J. Mater. Sci , Vol. 40, pp. 711-717, 2005.

[12] K. HIRANO – *Application of Eutectic Composites to Gas Turbine System and Fundamental Fracture Properties up to 1700 °C*. J. Eur. Ceram. Soc., Vol. 25, pp. 1191-1199, 2005.

[13] N. PIQUET - *Microstructures interconnectées dans des eutectiques à base d'oxydes réfractaires élaborés par solidification dirigée.* Doctorate thesis, Univ. Paris XII, 2006.

[14] L. PERRIÈRE - *Elaboration par solidification dirigée et comportement mécanique de céramiques eutectiques à base d'oxydes réfractaires. Rôle de la microstructure sur la fissuration et la déformation plastique à haute température.* Doctorate thesis, Univ. Paris-Est, 2008.

[15] L. MAZEROLLES, D. MICHEL, M. J. HYTCH - *Microstructures and Interfaces in Directionally Solidified Oxide–Oxide Eutectics.* J. Eur. Ceram. Soc., Vol. 25, pp. 1389–1395, 2005.

[16] G. GOUADEC, Ph. COLOMBAN, N. PIQUET, M. F. TRICHET, L. MAZEROLLES - *Raman/Cr^{3+} Fluorescence Mapping of a Melt-Grown Al_2O_3/$GdAlO_3$ Eutectic.* J. Eur. Ceram. Soc., Vol. 25, pp. 1447-1453, 2005.

[17] L. MAZEROLLES, N. PIQUET, M. F. TRICHET, M. PARLIER - *Microstructures and Interfaces in Melt-Growth Al_2O_3-Ln_2O_3 Based Eutectic Composites.* Adv. Sci. Techn., Vol. 45, pp. 1377-1384, 2006.

[18] L. MAZEROLLES, N. PIQUET, M. F. TRICHET, L. PERRIÈRE, D. BOIVIN, M. PARLIER - *New Microstructures in Ceramic Materials from the Melt for High Temperature Applications.* Aerospace Sci. Techn., Vol. 12, pp. 499–505, 2008.

[19] L. PERRIÈRE, R. VALLE, L. MAZEROLLES, M. PARLIER - *Crack Propagation in Directionally Solidified Eutectic Ceramics.* J. Eur. Ceram. Soc., Vol. 28, pp. 2337–2343, 2008.

[20] L. MAZEROLLES, L. PERRIÈRE, S. LARTIGUE-KORINEK, N. PIQUET, M. PARLIER - *Microstructures, Crystallography of Interfaces and Creep Behavior of Melt-Growth Composites*. J. Eur. Ceram. Soc., Vol. 28, pp. 2301–2308, 2008.

[21] L. MAZEROLLES, L. PERRIERE, S. LARTIGUE-KORINEK, M. PARLIER - *Creep Behavior and Related Structural Defects in Al_2O_3-Ln_2O_3 (ZrO_2) Directionally Solidified Eutectics (Ln = Gd, Er, Y)*. J. Eur. Ceram. Soc., Vol. 31, pp. 1219–1225, 2011.

[22] L. PERRIÈRE, R. VALLE, N. CARRÈRE, G. GOUADEC, Ph. COLOMBAN, S. LARTIGUE-KORINEK, L. MAZEROLLES, M. PARLIER - *Crack Propagation and Stress Distribution in Binary and Ternary Directionally Solidified Eutectic Ceramics*. J. Eur. Ceram. Soc., Vol. 31, pp. 1199–1210, 2011.

[23] J. GUIDEZ, F. X. NICOUL, P. JOSSO, R. VALLE - *Development of a Micro Gas Turbine Engine at Onera*. Proceedings 19th ISABE Conference (Int. Soc. Air Breathing Engines), September 7-11, 2009, Montréal, Canada, Paper n°ISABE-2009-1307, 2009.

[24] M. MIZUNO, T. YAMADA, T. NOGUCHI - *Phase Diagrams of the Systems Al_2O_3-Eu_2O_3 and Al_2O_3-Gd_2O_3 at High Temperatures.* Yogyo Kyokai Shi, Vol. 85, pp. 543-548, 1977.

[25] W. KURZ, D. J. FISHER - *Fundamentals of Solidification*. 3rd Edition, Trans Tech Publications, 1989.

[26] J. J. RASMUSSEN, R. P. NELSON - *Surface Tension and Density of Molten Al_2O_3*. J. Am. Ceram. Soc., Vol. 54, pp. 398-401, 1971.

[27] B. CHALMERS, H. E. LABELLE Jr., A. J. MLAVSKY - *Edge-Defined, Film-Fed Crystal Growth*. J. Crystal Growth, Vol. 13/14, pp. 84-87, 1972.

[28] H. E. LABELLE Jr. – *EFG, the Invention and Application to Sapphire Growth*. J. Crystal Growth, Vol. 50, pp. 8-17, 1980.

[29] D. A. JEREBTSOV, G. G. MIKHAILOV - *Phase Diagram of CaO-Al_2O_3 System.* Ceramics Int., Vol. 27, pp. 25-28, 2001.

[30] Y. HARADA, T. SUZUKI, K. HIRANO, N. NAKAGAWA, Y. WAKU – *Environmental Effects on Ultra-High Temperature Creep Behavior of Directionally Solidified Oxide Eutectic Ceramics.* J. Eur. Ceram. Soc., Vol. 25, pp. 1275-1283, 2005.

[31] A. H. HEUER - *Oxygen and Aluminum Diffusion in α-Al_2O_3: How Much do we Really Understand?* J. Eur. Ceram. Soc., Vol. 28, pp. 1495-1507, 2008.

[32] J. RAMIREZ-RICO, A. R. PINTO-GÓMEZ, J. MARTINEZ-FERNANDEZ, A. R. de ARELLANO-LÓPEZ, P. B. OLIETE, J. I. PEÑA, V. M. ORERA – *High-Temperature Plastic Behaviour of Al_2O_3–$Y_3Al_5O_{12}$ Directionally Solidified Eutectics.* Acta mater., Vol. 54, pp. 3107–3116, 2006.

[33] J. CASTAING, A. MUNOZ, D. GOMEZ GARCIA, A. DOMINGUEZ RODRIGUEZ - *Basal Slip in Sapphire (α-Al_2O_3).* Mater. Sci. Eng. A, Vol. 233, pp. 121-125, 1997.

[34] M. CASTILLO RODRÍGUEZ, J. CASTAING, A. MUÑOZ, P. VEYSSIÈRE, A. DOMÍNGUEZ RODRÍGUEZ - *Analysis of a Kink Pair Model Applied to a Peierls Mechanism in Basal and Prism Plane Slips in Sapphire (α-Al_2O_3) Deformed Between 200 °C and 1800 °C.* J. Am. Ceram. Soc., Vol. 91, pp. 1612-1617, 2008.

Acronyms

CMC (Ceramic Matrix Composite)
CVD (Chemical Vapor Deposition)
DSE (Directionally Solidified Eutectic)
EAG (Erbium Aluminum Garnet)
EBSD (Electron Back-Scattered Diffraction)
EHM (Equivalent Homogeneous Medium)
FEG-SEM (Field Emission Gun - Scanning Electron Microscopy)
GAP (Gadolinium Aluminum Perovskite)
HRTEM (High Resolution Transmission Electron Microscopy)
IMC (Intermetallic Matrix Composite)
IPF (Inverse Pole Figure)
MGC (Melt-Growth Composite)
MMC (Metal Matrix Composite)
PF (Pole Figure)
SAED (Selected Area Electron Diffraction)
SEM (Scanning Electron Microscopy)
TEM (Transmission Electron Microscopy)
UTS (Ultimate Tensile Stress)
YAG (Yttrium Aluminum Garnet)

AUTHORS

Michel Parlier, holding an Engineering Diploma from ENSCI (Ecole Nationale Supérieure de Céramiques Industrielles) and having graduated in Materials Science from the University of Paris, he received his Doctorate Degree in Metallurgy (Mechanical Behavior of Materials) from ENSMP (Ecole Nationale Supérieure des Mines de Paris) in 1984. Head of the High Temperature Composite Materials Unit at Onera (Composite Materials and Structures Department), he has been involved in the development of sintering techniques of ceramic powders with specific additives (hot-pressing, reaction bonding, hot isostatic pressing); Chemical Vapor Deposition (CVD) for densification of composites and coatings; Ceramic Matrix Composites (CMC) development (glass-ceramics, oxides and silicon carbide); Oxides derived from Sol-Gel; Silicon carbide derived from organosilicon precursors, low density fibrous thermal insulation; Melt-Growth Composites (MGC) processing routes; thermal, mechanical and microstructural characterizations.

Roger Valle, having Masters Degrees (Maîtrises) in Mathematics and Physics, and an Engineering Diploma from the Ecole Nationale Supérieure des Mines de Paris, and having graduated in Theoretical Solid State Physics from the University of Paris, he received his Doctorate Degree (Doctorat d'État ès Sc., Hab. Dir. Rech.) from the University of Lille. From 1973 to 1987, he was in charge of the development of instrumentation and *in situ* experimentation in materials science (electron-solid interaction, plastic deformation, fracture, recrystallization, texture …) in the High Voltage Electron Microscope Cnrs-Onera Laboratory (LP 12 8714). Since then, he works on the microstructural and mechanical aspects of deformation and failure of Metal Matrix Composites (MMC), Ceramic Matrix Composites (CMC), Intermetallic Matrix Composites (IMC) and Melt-Growth Composites (MGC) subjected to thermomechanical loadings (Composite Materials and Structures Department).

Loïc Perrière, obtained his Master's Degree in Materials Science and Engineering and his Engineering Diploma from the Institut National Polytechnique de Toulouse in 2005. He performed his doctorate work at Onera on directionally solidified eutectic ceramics and obtained his PhD from the University of Paris Est - Créteil in 2008. He currently works as a research scientist at the ICMPE (Institut de Chimie et des Matériaux Paris-Est, UMR 7182) on the development and manufacturing of amorphous metallic alloys.

Sylvie Lartigue-Korinek, obtained her PhD in Metallurgy and then her Doctorat d'État ès Sciences Physique-Chimie (Hab. Dir. Rech.) from the University of Paris-Sud (Orsay). Since 1986 she has been a Cnrs researcher and has worked in the field of structure and properties of interfaces, with a particular emphasis on the role of grain boundary chemistry on deformation micromechanisms in metals and ceramics. She currently works at ICMPE (Institut de Chimie et des Matériaux Paris-Est, UMR 7182) in the group "Métaux et Céramiques à Microstructures Contrôlées".

Léo Mazerolles is Director of Research at Cnrs. Graduated as an Engineer from the Ecole Nationale Supérieure de Chimie de Lille (1979), with a PhD degree from University Paris VI (1982) and a Research Habilitation Thesis (Thèse d'État) in Physical Sciences from University Paris VI (1986), he is a researcher in physicochemistry of solids and inorganic materials. One of his main fields of research concerns ceramic oxide materials and more particularly the synthesis and study of microstructures (morphology, size, interfaces). He studies relationships between properties and structural/microstructural features of refractory oxides. Since 2007, he manages the "Metals and ceramics" team at ICMPE (Institut de Chimie et des Matériaux Paris-Est, UMR 7182) in Thiais.